**Synthesis, characterization, X-ray structural determination and theoretical study of the complexes [RuCp(8MTT-$\kappa S$)LL'] (8MTT = 8-methylthio-theophyllinate; L,L' = PTA, mPTA; L = mPTA, L' = PPh$_3$; PTA = 1,3,5-triaza-7-phosphaadamantane, mPTA = N-methyl-1,3,5-triaza-7-phosphaadamantane).**

Lazhar Hajii, Vicente Jara-Pérez, Cristobal Saraiba-Bello, Gaspar Segovia-Torrente, Manuel Serrano-Ruiz, Antonio Romerosa[*]

[a] *Área de Química-Física y Química Inorgánica, Facultad de Ciencias Experimentales, Universidad de Almería, 04071 Almería – Spain*

## Graphical Abstract

Two new thiopurine-$\kappa S$-complexes, [RuCp(8MTT-$\kappa S$)(mPTA)(PPh$_3$)]$^+$ (**1**) and [RuCp(8MTT-$\kappa S$)(mPTA)$_2$]$^{2+}$ (**2**) were synthesized and characterized by single crystal X-ray diffraction. The thiopurine coordination was evaluated by DFT theoretical methods by study of the isomer complexes in gas phase and water.

[RuCp(8MTT-$\kappa S$)(PTA)$_2$]     [RuCp(8MTT-$\kappa N7$)(PTA)$_2$]
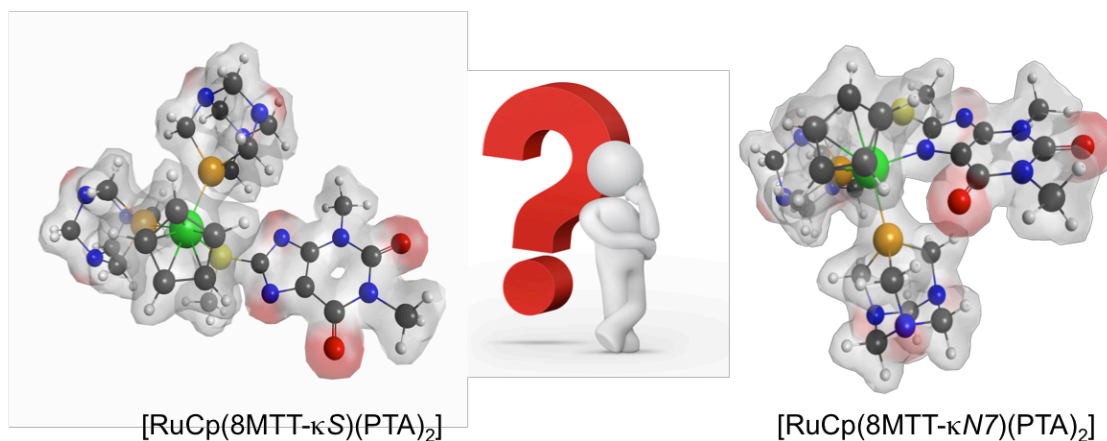
**Abstract**

The complexes [RuCp(8MTT-κ*S*)LL'] and [RuCp(8MTT-κ*N7*)LL'] (8MTT = 8-methylthio-theophyllinate; L,L' = PTA, mPTA; L = mPTA, L' = PPh$_3$; PTA = 1,3,5-triaza-7-phosphaadamantane, mPTA = N-methyl-1,3,5-triaza-7-phosphaadamantane) have been investigated by DFT theoretical methods. Structures, infrared spectra and thermodynamical properties in gas phase, water and ethanol of the studied complexes have been determined at B3LYP/DZVP level of theory. Complexes [RuCp(8MTT-κ*S*)(PTA)$_2$] and [RuCp(8MTT-κ*S*)(mPTA)(PPh$_3$)]$^+$ are slightly stabilized by favourable Gibbs free energy respect to [RuCp(8MTT-κ*N7*)(PTA)$_2$] and [RuCp(8MTT-κ*N7*)(mPTA)(PPh$_3$)]$^+$ in gas phase while in water and ethanol the calculated Gibbs free energy showed that the 8MTT-κ*S*-complexes are quite more stable than the corresponding 8MTT-κ*N7*-complexes. However, the [RuCp(8MTT-κ*N7*)(mPTA)$_2$]$^{2+}$ is more stable than the corresponding κ*S*-complex in gas phase while in water remains less stable. These theoretical results are in agreement with obtained until now experimental results as two new 8MTT-κ*S*-complexes, [RuCp(8MTT-κ*S*)(mPTA)(PPh$_3$)](CF$_3$OSO$_2$) (**1**) and [RuCp(8MTT-κ*S*)(mPTA)$_2$]Cl(CF$_3$OSO$_2$)·1.5H$_2$O (**2·1.5H$_2$O**) were synthesized and characterized by single crystal X-ray diffraction.

**Keywords:** Ruthenium, water soluble complexes, PTA derivatives, thio-purines, theoretical studies, DFT.

**Introduction**

   A huge number of metal compounds of wide structural diversity have been tested and some of them found to be therapeutic agents for cancer treatment [1] after the discovery of the anticancer properties of *cis*platin [2] in the sixties by Rosenberg. Still now *cis*platin and its parent analogues are among the most widely used chemotherapeutic agents [3] but they present a few drawbacks like drug resistance [4]. Ruthenium complexes are promising anticancer agents [5] and two of them, NAMI-A [6] and KP1019 [7] are currently under clinical trials, for the treatment of metastatic and colorectal cancers, respectively. On the base of the promising results we have obtained on platinum [8,9] and ruthenium [10]

complexes containing the water soluble phosphine PTA and its derivative mPTA (PTA = 1,3,5-triaza-7-phosphaadamantane; mPTA = *N*-methyl-1,3,5-triaza-7-phosphaadamantane) we planned the substitution of the chloride ligand in [RuCpCl(PR$^1_3$)(PR$^2_3$)] complexes (PR$^1_3$ = PPh$_3$; PR$^2_3$ = PTA) by a thiopurine. The aims were enhance the antiproliferative activity of the parent complexes obtained with thiopurines and obtaining additional information on the interaction of ruthenium complexes with purines. The obtained water soluble ruthenium complexes [RuCp(X)(PR$^1_3$)(PR$^2_3$)] (X = 8-thio-teophyllinate (TTH), 8-methyl-thio-teophyllinate (8MTT), 8-benzyl-thio-theophyllinate (8BzTT) and binuclear ruthenium complexes [{RuCp(L)(L')}$_2$-$\mu$-(Y-$\kappa$*N7,N´7*)] (Y = bis-thiopurines-bis(S-8-thiotheophyllinate)methane (MBTT$^{2-}$), 1,2-bis(S-8-thiotheophyllinate)ethane (EBTT$^{2-}$), 1,3-bis(S-8-thiotheophyllinate)propane (PBTT$^{2-}$) with two coordinated PTA ((PR$^1_3$ = PR$^2_3$ = PTA) or one PPh$_3$ and one PTA (PR$^1_3$= PPh$_3$; PR$^2_3$ = PTA) showed an improved antiproliferative activity on *cis*platin-sensitive T2 and *cis*platin-resistant SKOV3 model cell lines than those for starting compounds [11].

Remarkably, the obtained complex [RuCp(8MTT-$\kappa$*S*)(PTA)$_2$] contains the ligand 8MTT but coordinated by its thio-S atom to the ruthenium instead of the purine-N7 atom, which was the expected coordination position.  Also, this complex was the first example of a single-S-coordinate thio-ether-amine and S-coordinated-thiopurinate. These results open the possible use of this kind of complexes for a different to that known activation of thio-ethers that could provide new thio-derivatives by catalytic procedures.

To achieve the possible reasons for this new and singular coordination of the 8MTT to the metal, which could be a normal reactivity for thiopurines against complexes [RuCpCl(PR$^1_3$)(PR$^2_3$)], a theoretical study was carried out. The suggestions afforded by the analysis of the theoretical results suggested that the S-coordination is the most stable for the 8MTT ligand and therefore it was checked experimentally. The complexes [RuCp(8MTT-$\kappa$*S*)(PPh$_3$)(mPTA)](CF$_3$SO$_3$) (**1**) and [RuCp(8MTT-$\kappa$*S*)(mPTA)$_2$]Cl(CF$_3$SO$_3$)·**1.5H$_2$O** (**2·1.5H$_2$O**) were characterized by elemental analysis, NMR, IR and single crystal X-ray diffraction.

**Experimental**

**Synthesis of [RuCp(8MTT-κ*S*)(PPh₃)(mPTA)](CF₃SO₃) (1).** The ligand 8MTTH (30.2 mg, 0.13 mmol) and KOH (7.5 mg, 0.13 mmol) were introduced into 10 mL of EtOH and stirred at room temperature for 15 minutes. The complex [RuCpCl(PPh₃)(mPTA)])(CF₃SO₃) (97.3 mg, 0.12 mmol) was added and after 10 min the resulting mixture was kept at refluxing for 4 h. The obtained solution was cooled, filtered and concentrate at 2 mL. A yellow precipitated was obtained by addition of 5 mL of Et₂O, which was filtered, washed with Et₂O (2 x 2 mL) and vacuum dried. Crystals adequate for single crystal X-ray diffraction were obtained by slow recrystallization from an EtOH solution at room temperature. Yield powder: 0.084 g, 66 %. Yield crystals: 0.059 g, 46 %.

**Synthesis of [RuCp(8MTT-κ*S*)(mPTA)₂]Cl(CF₃SO₃)·1.5H₂O (2·1.5H₂O).** Into 10 mL of H₂O was added 8MTTH (27.6 mg, 0.122 mmol) and KOH (6.3 mg, 0.112 mmol). After 15 min the complex [RuCpCl(mPTA)₂](CF₃SO₃)₂ (86 mg, 0.102 mmol) was incorporated. The resulting mixture was refluxed for 4 h., cooled at room temperature, the solvent reduced to 1 mL and 2 mL of EtOH added. A yellow precipitate was obtained when 10 mL of Et₂O was poured into the solution, which was filtered, washed with cool EtOH (1 x 2mL), Et₂O (2 x 2 mL) and vacuum dried. Crystals useful for structural single crystal X-ray determination were obtained by slow evaporation from an ethanolic solution at room temperature. Yield powder: 0.072 g, 75 %. Yield crystals: 0.063 g, 65 %.

**X-ray structure determinations.**

Data of compounds **1** and **2·1.5H₂O** were collected on a Bruker APEX CCD diffractometer (XDIFRACT service of the University of Almería) using graphite monochromated Mo-Kα radiation (λ = 0.7107 Å) at 150 K. The crystal parameters and other experimental details of the data collections are summarized in Table 1. The structures were solved by direct methods SIR92 [12] and refined by full-matrix least squares methods with SHEL-XTL [13] and refined by least-squares procedures on $F^2$ and final geometrical calculations

and graphical manipulations were carried out with the SHEL-XTL package [18].
A disordered solvent molecule of $H_2O$ was found in **2·1.5H₂O** and refined
isotropically. All the non-hydrogen-non-disordered atoms were refined with
anisotropic atomic displacement parameters. All hydrogen atoms, excepting for
disordered water molecules, were included in calculated positions and refined
using a riding model.

Table 1. Crystallographic data for **1** and **2·1.5H₂O**

|  | **1** | **2·1.5H₂O** |
|---|---|---|
| Chemical Formula | $C_{39}H_{44}F_3N_7O_5P_2RuS_2$ | $C_{28}H_{47}ClF_3N_{10}O_{6.5}P_2RuS_2$ |
| FW (g·mol⁻¹) | 974.95 | 947.33 |
| Crystal system | Monoclinic | Triclinic |
| Space group | P 2(1)/c | P -1 |
| a (Å) | 10.618(15) | 15.375(5) |
| b (Å) | 19.886(3) | 17.753(5) |
| c (Å) | 19.664(3) | 17.894(5) |
| $\alpha$ (deg) | 90.000 | 109.084(5) |
| $\beta$ (deg) | 92.249(4) | 113.249(5) |
| $\gamma$ (deg) | 90.000 | 98.157(5) |
| Z | 4 | 4 |
| V (Å³) | 4149(2) | 4029(2) |
| $d_{calcd}$ (g·cm⁻³) | 1.561 | 1.562 |
| $\mu$(Mo K$\alpha$)/cm⁻¹ | 6.22 | 7.06 |
| F(000) | 2000 | 1936 |
| Crystal size/mm | 0.183×0.135×0.095 | 0.125×0.098×0.073 |
| θmin-θmax/deg | 1.46 – 23.25 | 1.28 – 24.40 |
| hkl ranges | $-11 \leq h \leq 11$ <br> $-22 \leq k \leq 20$ <br> $-21 \leq l \leq 20$ | $-17 \leq h \leq 17$ <br> $-20 \leq k \leq 18$ <br> $-20 \leq l \leq 17$ |
| Measured reflns | 19019 | 20732 |
| Unique reflns | 5944 | 13040 |
| Obsd reflns [I≥2σ(I)] / number of variables | 4646 /537 | 8143/996 |
| Goodness of fit | 0.945 | 0.985 |
| R [I>2σ(I)] | $R_1 = 0.0353$ | $R_1 = 0.0674$ |

| R (all data) | $R_{w2}$ = 0.0743 | $R_{w2}$ = 0.1922 |
|---|---|---|
| | $R_1$ = 0.0488 | $R_1$ = 0.0995 |
| | $R_{w2}$ = 0.0938 | $R_{w2}$ = 0.2190 |

**Theoretical procedures**

Calculations were perfomed by using the GAMESS program [14,15]. Structures for complexes [RuCp(8MTT-$\kappa S$)LL'] and [RuCp(8MTT-$\kappa N7$)LL'] were fully optimized at the B3LYP level which incorporates Becke's three-parameter hybrid functional [16] and the Lee, Yang and Parr correlation functional [17]. The DZVP basis set was used as it is the largest one available for ruthenium [18]. The obtained crystal structures for $\kappa S$-8MTT-complexes were used as starting point for the optimization of the rest of studied [RuCp(8MTT-$\kappa S$)LL'] complexes, which were used later as starting point for obtaining the corresponding $\kappa N7$-8MTT-complexes initial structural geometries. These starting structures were shaped by the Avogadro program [19]. The structures of S-methyl-8-thiotheopylline (8MTTH) and its anion S-methyl-8-thiotheopyllinate (8MTT) were optimized at B3LYP level of theory with Pople 6-311(d,p)++ basis set [20,21,22]: a valence triple zeta basis set with polarization and diffuse on all atoms. The nature of the stationary points were verified by computation of vibrational frequencies, which were also used for the computation of molecular partition functions and 298 K thermal contributions to free energies, following the usual rigid-rotator harmonic-oscillator ideal-gas approximation. Solvation free energies, $\Delta G_{solv}$, in water and ethanol were calculated using the conductor polarizable continuum model (CPCM) [23,24,25]. The solvent cavity was constructed based on the van der Waals radii of the atoms, taking 2.30 Å for Ru radius [26]. A single point calculation was done to obtain $\Delta G_{solv}$ by using the resulting equilibrium geometry of the complexes in the gas phase. The Gibbs free energies of the complexes in solution were determined by $G_{sln} = G_{gas} + G_{solv} + RTln(RT/P)$ and using the final term for conversion from the gas-phase standard state (defined by *T* and *P*) to the solution-phase standard state of 1 M [27]. The IR frequencies were calculated with B3LYP functional. To our knowledge no scaling factor is available for DZVP

basis set and for this reason the scaling factor (0.96) determined for the double zeta basis set 6-31G* was used [28]. Molecular orbitals isosurfaces and electrostatic potential maps have been drawn with Wxmacmolplt software [29].

## Results and discussions

### Synthesis of 1 and 2·1.5H₂O

Initially, the spectroscopic data suggested that both complexes **1** and **2·1.5H$_2$O** (Supporting Information) are similar to other previously reported 8-MTT metal complexes. As observed for complex [RuCp(8-MTT-$\kappa S$)(PTA)$_2$], the IR spectrum of complexes **1** and **2·1.5H$_2$O** do not show any characteristic $\nu$(N-H) absorption band but absorptions for $\nu$(C6=O+C2=O) and $\nu$(C=C+C=N) in the range found for 8-MTT-complexes in which the purine is bonded to the metal by the imidazolic N7 atom [17,18,22,23a]. $^1$H, $^{13}$C and $^{31}$P NMR spectra of **1** showed a single pattern, excluding the formation of two coordination isomers (S and N7 coordinated MTT). The $^1$H NMR displayed the expected signals for a Cp, a PTA, a PPh$_3$ and an 8-MTT. It is important to point out that the singlet for S-CH$_3$ at 2.40 ppm is far from that for the parent [RuCp(8-MTT-$\kappa S$)(PTA)$_2$] (2.75 ppm), suggesting a possible coordination of the 8-MTT by the imidazolic N7 atom [11]. Nevertheless, the $^{13}$C{$^1$H} NMR of **1** shows that the S-CH$_3$ arises at 14.52 ppm that is close to that for [RuCp(8-MTT-$\kappa S$)(PTA)$_2$] (14.15 ppm) and for free 8-MTTH (14.00 ppm) [22,23]. The $^{31}$P{$^1$H} NMR spectrum showed a doublet at 46.57 ppm due to the P$_{PPh_3}$ and other at -17.53 ppm corresponding to the P$_{mPTA}$, which are similar to those found for [RuCpCl(mPTA)(PPh$_3$)](CF$_3$SO$_3$) (-15.38 ppm, 46.31 ppm)) [10]. Therefore, from the NMR spectroscopic data of **1** is not possible to propose indisputably the coordination position to the metal of the 8-MTT. Finally, it was possible to obtain crystals of **1** good enough for obtaining its structure by single crystals X-ray diffraction. The structure of **1** is constituted by a distorted octahedral ruthenium bonded to a $\eta^5$-Cp, two PTA by the P atom and one 8-MTT coordinated to the metal by the S atom instead of the N7 imidazolic atom (Figure 7). It is important to stress that the S is still bonded to both the C8 and CH$_3$. Therefore this is the second example of a metal complex containing a coordinated mono-thio-ethereal group.

The complex [RuCp(8-MTT-$\kappa S$)(mPTA)$_2$]Cl(CF$_3$SO$_3$)·1.5H$_2$O (**2·1.5H$_2$O**) was obtained by a procedure similar to that used for **1**. Reaction of 8-MTTH with KOH and after that with [RuCpCl(mPTA)$_2$](CF$_3$SO$_3$)$_2$ in water. The IR spectrum showed the typical bands for a coordinated thiopurine and the lack of $\nu$(N7H) absorption but also an intense broad band for lattice H$_2$O was observed at 3420 cm$^{-1}$. The $^1$H NMR is constituted by the characteristic signals for mPTA, Cp and the thiopurine. The chemical shift for the S-CH$_3$ signal (2.13 ppm) is far to high field from that for **1** and [RuCp(8-MTT-$\kappa S$)(PTA)$_2$], discussed previously, while in its $^{13}$C{$^1$H} NMR the chemical shifts of S-CH$_3$ arises at 14.20 ppm, a similar chemical shift than that observed for complex **1** (14.52 ppm) and [RuCp(8-MTT-$\kappa S$)(PTA)$_2$] (14.15 ppm). The C8-S arises in **2** at 158.93 ppm practically at the same chemical shift than that in **1** (157.75 ppm) and in [RuCp(8-MTT-$\kappa S$)(PTA)$_2$] (158.89 ppm). In the $^{31}$P{$^1$H} NMR a singlet comes at -10.83 ppm that is practically the same chemical shift than that observed for [RuCpCl (mPTA)$_2$](CF$_3$SO$_3$)$_2$ (-10.74 ppm) [10]. The crystal structure of complex **2·1.5H$_2$O** (Figure 9) showed as the complex is constituted by a 8-MTT ligand bonded to the metal by the S atom.

**Computational study of the ligands 8MTTH and 8MTT**

As an initial step the electron donor properties of the ligand 8MTTH and its corresponding thiolate (8MTT) were determined. Their optimized structures and selected bonds lengths and angles are displayed in Figure 1. It is interesting to point out that the theoretical results show that the deprotonation of the N7 purine atom leads to the reduction of the C8-N7 bond from 1.36 Å to 1.32 Å while the C8-N9 bond length growths from 1.33 Å to 1.37 Å, increasing the electronic density on the C8-N7 bond. Both molecules 8MTTH and 8MTT are essentially planar with similar imidazole/pyrimidine-mean plane angle (respectively 0.22º and 0.15º).
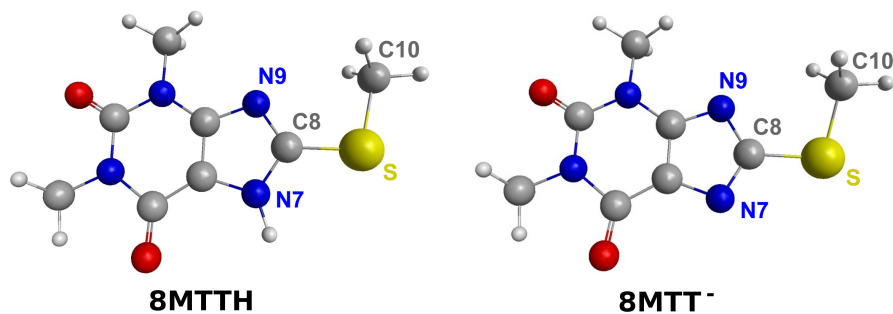
Figure 1. B3LYP/6-311(d,p)++ optimized structures of 8MTTH and 8MTT. Selected Bond Distances (Å) and Angles (deg). 8MTTH: C10-S = 1.8260, S-C8 = 1.7575, C8-N7 = 1.3612, C8-N9 = 1.3288, C10-S-C8 = 101.28, S-C8-N7 = 126.15, S-C8-N9 = 121.86; 8MTT: C10-S = 1.8234, S-C8 = 1.7825, C8-N7 = 1.3227, C8-N9 = 1.3701, C10-S-C8 = 99.65, S-C8-N7 = 123.71, S-C8-N9 = 118.22.

The electronic structures of 8-MTTH and 8-MTT was analysed by the Chemissian software [30]. The resulting isosurfaces and electrostatic potential maps of 8-MTT and 8-MTTH are shown in Figure 2. For both molecules the HOMO orbitals have mainly a character π, being constituted by the p-orbitals of S, N7 and N9 (respectively 20%, 9% and <0.5% for 8-MTT; 20%, 4% and 1% for 8MTTH). The largest electron density is located on the S atom in both molecules.

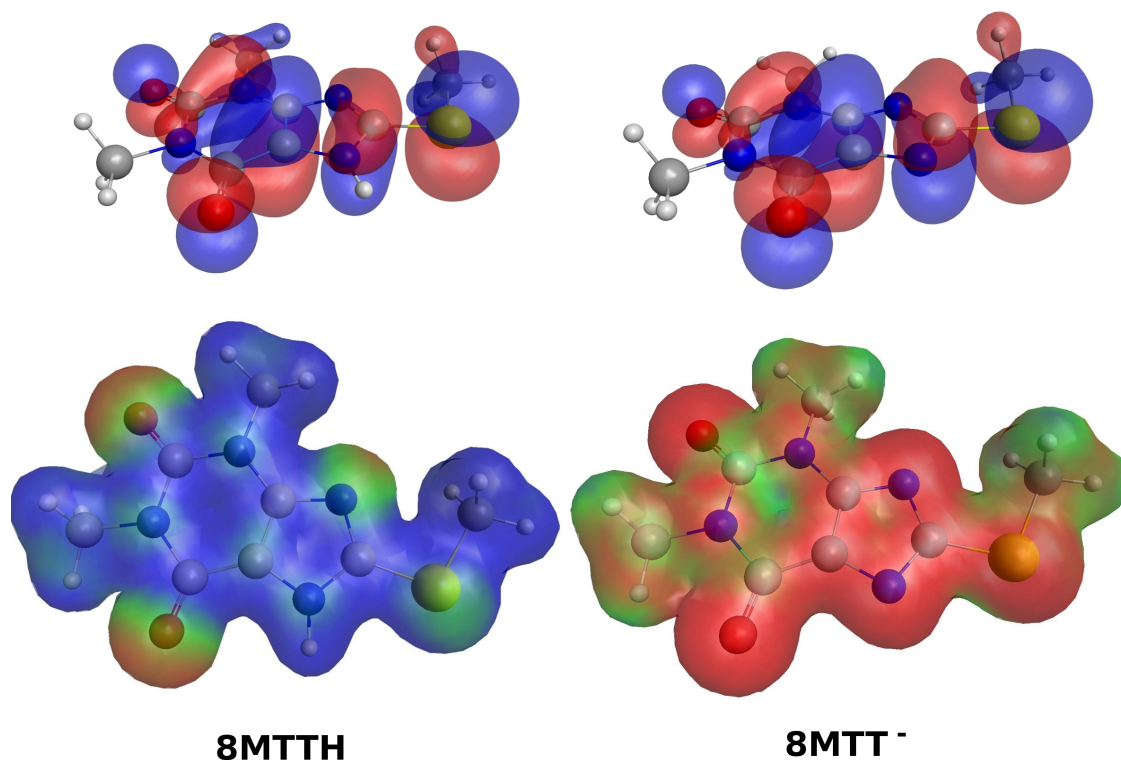**8MTTH**                                    **8MTT** -

Figure 2. HOMO of 8MTTH (left top) and 8MTT (right top). Isosurfaces correspond to 0.02 au. Electrostatic potential maps of 8MTTH (left bottom) and 8MTT (right bottom). Electrostatic potential maps are superimposed over total electronic density surface (0.02 au). Maximum electrostatic potential plot is 0.08 au. Colours represent, red negative, blue positive and green zero electrostatic potential.

It is important to point out that, as expected, the negative charge generated by the N7 deprotonation is mainly delocalized on the purine ring but concentrated not only on the imidazolic nitrogens but also on the S atom ($S_{Mulliken\ charges}$ = -0.119 au; $N7_{Mulliken\ charges}$ = -0.187 au). Therefore, according to the electron density distribution the 8MTT ligand could act as an electron donor through the N7, as expected and observed previously, but also through the thioether-S atom.

**Computational study of the ruthenium complexes**

The optimized molecular geometries of complexes [RuCp(8MTT-κ*S*)(mPTA)(PPh₃)]⁺, [RuCp(8MTT-κ*N7*)(mPTA)(PPh₃)]⁺, [RuCp(8MTT-κ*S*)(mPTA)₂]²⁺, [RuCp(8MTT-κ*N7*)(mPTA)₂]²⁺, [RuCp(8MTT-κ*S*)(PTA)₂] and [RuCp(8MTT-κ*N7*)(PTA)₂] are shown in Figure 3. Cartesian coordinates of the optimized structures of these complexes are included in supporting information.
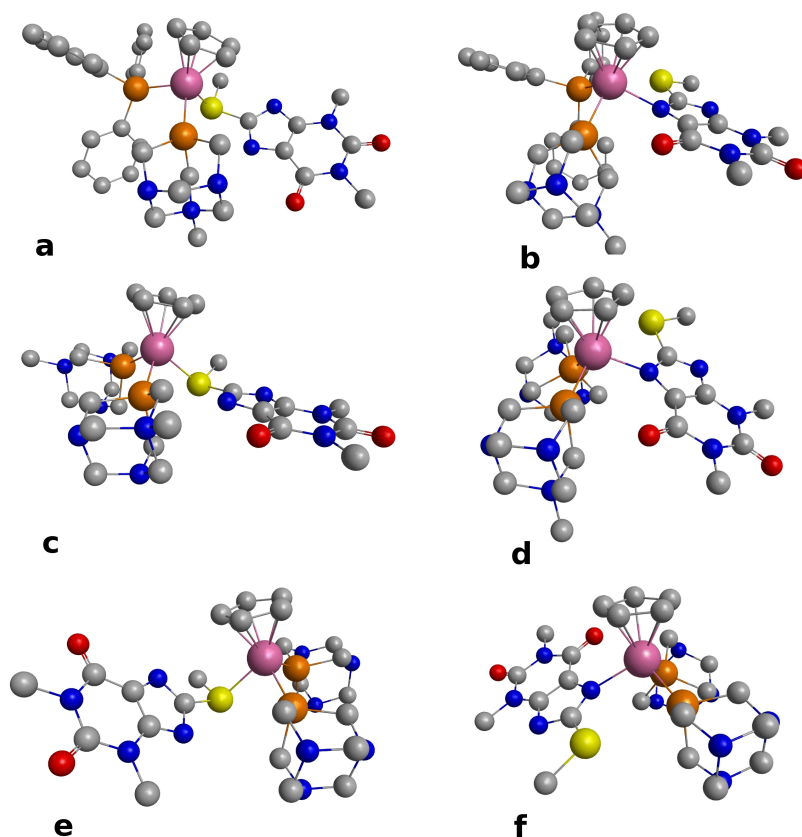


Figure 3. B3LYP/DZVP optimized structures of (a) [RuCp(8MTT-κ*S*)(mPTA)(PPh₃)]⁺, [RuCp(8MTT-κ*N7*)(mPTA)(PPh₃)]⁺ , (b) [RuCp(8MTT-κ*S*)(mPTA)₂]²⁺, [RuCp(8MTT-κ*N7*)(mPTA)₂]²⁺ (c) [RuCp(8MTT-κ*S*)(PTA)₂] and [RuCp(8MTT-κ*N7*)(PTA)₂]. For the sake of clarity hydrogens are not shown.

The theoretical study showed that in gas phase the κ*S*-complexes containing PTA are somewhat more stables than the corresponding κ*N*-ones while the reverse stability was found in complexes with mPTA. To obtain experimental support for this finding the synthesis of the theoretically studied complexes was accomplished. Although pure compounds were obtained for all checked

combinations of PTA, mPTA and PPh₃ phosphines in the {CpRuLL´} moiety, only two of them were possible to be characterized by single crystal X-ray analysis (see below). In both new obtained complexes the 8MTT ligand is bonded to the metal by the S atom. The calculated structures for synthesized $\kappa S$-complexes are in good agreement with their X-ray structures, although optimized Ru-P and Ru-S bond lengths are approximately 5 % larger than crystalline ones. Similar deviations were found in bibliography for Ru(II)-complex structures when calculated at B3LYP/DZVP and B3LYP/LANL2DZ levels [31].

Selected bond lengths and angles for optimized structures of complexes [RuCp(8MTT-$\kappa N7$)(mPTA)(PPh₃)]⁺, [RuCp(8MTT-$\kappa N7$)(mPTA)₂]²⁺ and [RuCp(8MTT-$\kappa N7$)(PTA)₂] are shown in Table 2. The three complexes show a similar piano stool structure in which the purines are basically planar. It is interesting to stress that the disposition of the purine with respect to the Cp changes significantly from [RuCp(8MTT-$\kappa N7$)(mPTA)(PPh₃)]⁺ (purine-plane/Cp plane = 10.55º) to [RuCp(8MTT-$\kappa N7$)(mPTA)₂]²⁺ (purine-plane/Cp plane = 28.66º) and [RuCp(8MTT-$\kappa N7$)(PTA)₂] (purine-plane/Cp plane = 53,20º).

Table 2. Selected Bond Distances (Å) and Angles (deg) for calculated structures for [RuCp(8MTT-$\kappa N7$)(mPTA)(PPh₃)]⁺ (A), [RuCp(8MTT-$\kappa N7$)(mPTA)₂]²⁺ (B) and [RuCp(8MTT-$\kappa N7$)(PTA)₂] (C).

|  | A | B | C |
|---|---|---|---|
| Ru1 – P1 | 2.3537 | 2.3473 | 2.3672 |
| Ru1 – P2 | 2.4581 | 2.3814 | 2.3769 |
| Ru1 – N7t | 2.2791 | 2.2465 | 2.2435 |
| Ru1-Cp(centroid) | 1.917 | 1.929 | 1.932 |
| C8t – N7t | 1.3553 | 1.3593 | 1.3487 |
| C5t – N7t | 1.4189 | 1.4128 | 1.4109 |
| P1 – Ru1 – P2 | 91.82 | 96.59 | 93.98 |
| P1 – Ru1 – N7t | 93.43 | 89.67 | 90.76 |
| P2 – Ru1 – N7t | 104.78 | 102.73 | 103.89 |

| | | | |
|---|---|---|---|
| C8t – N7t – Ru1 | 124.99 | 123.86 | 130.50 |
| C5t – N7t – Ru1 | 127.60 | 133.37 | 125.77 |

The vibrational frequencies of the complexes calculated in gas phase were positive without any imaginary term, confirming that optimized molecular geometries correspond to the minima of the potential energy surface. Additionally, the analysis of the vibrational frequencies provides the Gibbs energy values, G, and the theoretical infrared spectra of the complexes that will be discussed later. The HOMO and LUMO orbitals of [RuCp(8-MTT-$\kappa S$)(mPTA)(PPh$_3$)]$^+$ and [RuCp(8-MTT-$\kappa N7$)(mPTA)(PPh$_3$)]$^+$ are shown in Figure 4. The HOMO for the $\kappa S$-complex is mainly constituted by the 8-MTT-HOMO-orbitals that slightly overlaps through one of the S lobes (4 % contribution) with one of the Ru-d orbitals (3 % contribution). Therefore, the metal would be weakly bonding to the ligand through the Ru-S. The HOMO for [RuCp(8-MTT-$\kappa N7$)(mPTA)(PPh$_3$)]$^+$ is constituted similarly to the parent 8MTT-$\kappa S$-complex. Nevertheless, the $\kappa N7$-complex-HOMO has a nodal plane between the Ru-d and N7-p-orbital, and therefore the resulting Ru-N7-bond-orbital has an antibonding character.
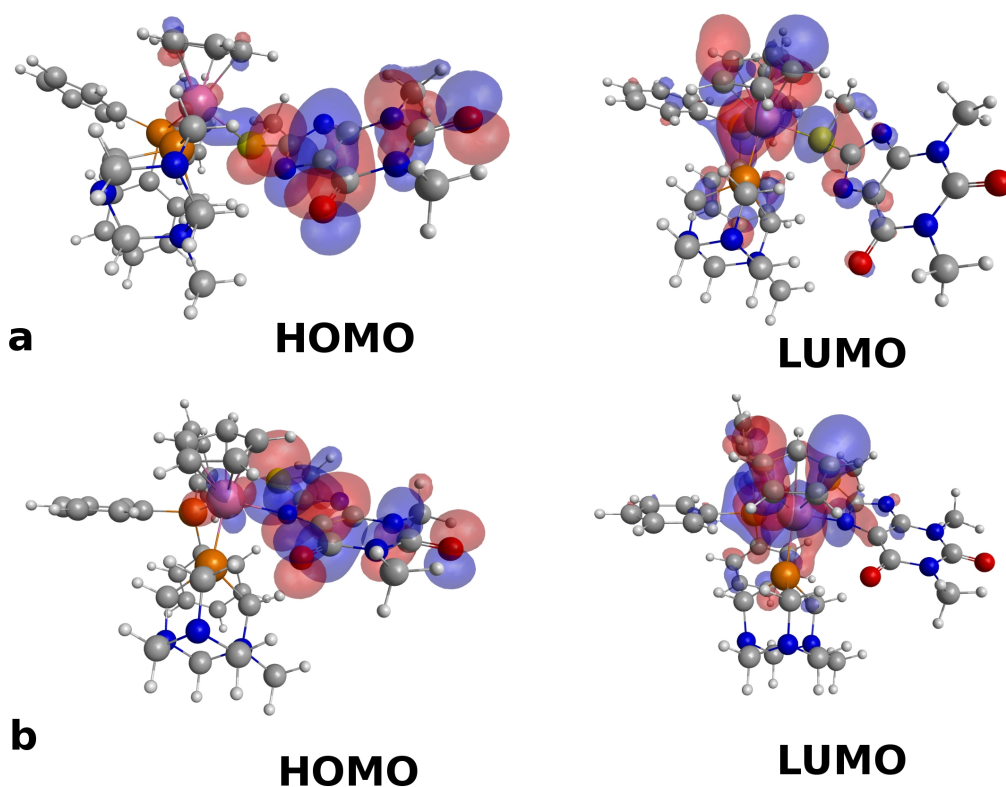
Figure 4. HOMO and LUMO of [RuCp(8-MTT-κ*S*)(mPTA)(PPh₃)]⁺ (a) and [RuCp(8-MTT-κ*N7*)(mPTA)(PPh₃)]⁺ (b).

The LUMO orbitals of [RuCp(8-MTT-κ*S*)(mPTA)(PPh₃)]⁺ and [RuCp(8-MTT-κ*N7*)(mPTA)(PPh₃)]⁺ are similar, being the main contribution to the LUMO the Cp-π orbital and in minor grade the Ru-d orbitals and triphenylphosphine-P-p orbitals. The orbital energies and composition in terms of fragments contributions for the most significant frontier molecular orbitals are shown in Table 3.

Table 3. Energies, occupancies and percentage composition of the HOMO and LUMO of the complexes [RuCp(8-MTT-κ*S*)(mPTA)(PPh₃)]⁺ and [RuCp(8-MTT-κ*N7*)(mPTA)(PPh₃)]⁺ in terms of Ru, Cp, 8MTT, mPTA and PPh₃ fragments.

| [RuCp(8-MTT⁻κ*S*)(mPTA)(PPh₃)]⁺ | | | | | | | [RuCp(8-MTT⁻κ*N7*)(mPTA)(PPh₃)]⁺ | | | | | | |
| MO | Occ | E(eV) | Ru | Cp | 8MTT | mPTA | PPh₃ | Occ | E(eV) | Ru | Cp | 8MTT | mPTA | PPh₃ |
|---|---|---|---|---|---|---|---|---|---|---|---|---|---|---|
| HOMO-4 | 2 | -8.629 | 10 | 1 | 83 | 5 | | 2 | -8.729 | 31 | 2 | 54 | 5 | 7 |
| HOMO-3 | 2 | -8.604 | 9 | 3 | 84 | 2 | 2 | 2 | -8.411 | 41 | 7 | 38 | 9 | 5 |
| HOMO-2 | 2 | -8.542 | 45 | 14 | 21 | 9 | 10 | 2 | -8.223 | 56 | 10 | 23 | 7 | 4 |
| HOMO-1 | 2 | -8.414 | 52 | 11 | 26 | 8 | 3 | 2 | -7.913 | 61 | 16 | 8 | 4 | 11 |
| HOMO | 2 | -7.040 | 4 | 2 | 94 | | | 2 | -7.208 | 4 | | 94 | | |
| LUMO | 0 | -4.117 | 42 | 21 | 12 | 1 | 24 | 0 | -3.687 | 47 | 24 | 7 | 2 | 20 |
| LUMO+1 | 0 | -3.959 | 36 | 20 | 3 | 16 | 24 | 0 | -3.581 | 36 | 19 | 1 | 16 | 27 |
| LUMO+2 | 0 | -3.608 | 6 | 3 | | 1 | 89 | 0 | -3.467 | 8 | 4 | | | 84 |
| LUMO+3 | 0 | -3.502 | 2 | | | | 96 | 0 | -3.306 | | | | 2 | 96 |
| LUMO+4 | 0 | -3.464 | 1 | | | 3 | 95 | 0 | -3.129 | 2 | | | 3 | 94 |

In κ*N7*-8MTT-complex HOMO-3 and HOMO-4 orbitals show a higher contribution from the Ru-d orbitals than those in 8MTT-κ*S*-complexes. The LUMO+2, LUMO+3 and LUMO+4 are mainly located on the triphenylphosphine ligand in the complexes [RuCp(8-MTT-κ*S*)(mPTA)(PPh₃)]⁺. Similar conclusions can be obtained from the shape and composition of the complexes [RuCp(8MTT-κ*S*)(mPTA)(PPh₃)]⁺ and [RuCp(8MTT-κ*N7*)(mPTA)(PPh₃)]⁺ (the HOMO and LUMO orbitals of [RuCp(8-MTT-κ*S*)(mPTA)₂]²⁺, [RuCp(8-MTT-κ*S*)(mPTA)₂] are included in supplementary material). Therefore, in gas phase the electronic structures of the 8MTT-κ*S*- and 8MTT-κ*N7*-complexes containing mPTA are similar and no significant reasons for the preferred coordination through S is drawn from them.

It is important to stress that the crystal structure of [RuCp(8MTT-κ*S*)(PTA)₂] was obtained in aqueous media. Therefore to know the possible influence of the solvent in the coordination position of the ligand 8MTT in the studied complexes, the Gibbs free energies of the 8MTT-κ*S*- and 8MTT-κ*N7*-complexes were calculated also in water at B3LYP/DZVP level of theory. Nevertheless, EtOH was used for the synthesis of the complexes **1** and **2** that also displayed the 8MTT-κ*S* coordination to the metal. Therefore additional information on how the EtOH could affect the coordination of the thio-purine is needed and a theoretical study with this solvent was made. The molecular optimization in

water and ethanol was calculated by using the CPCM continuum solvent model of Tomasi and coworkers [28,29]. Gibbs free energies in solution of $\kappa S$-8MTT-complexes have been obtained by taking $\kappa N7$-8MTT-complexes in solution as reference ($G_{sln}(\kappa N7)=0$) and using the formula $\Delta G_{sln}= \Delta G_{gas}+\Delta\Delta G_{solv}$ ($\Delta G_{gas} = G_{gas}(kS)-G_{gas}(\kappa N7)$; $\Delta\Delta G_{solv} = \Delta G_{solv}(\kappa S)-\Delta G_{solv}(\kappa N7)$) (Table 4).

Table 4. $\Delta G_{gas}$, $\Delta G_{solv}$, $\Delta G_{sln}$ of the studied $\kappa S$- and $\kappa N7$-8MTT-complexes in water and ethanol.

| | $\Delta G_{gas}$ kcal/mol | $\Delta G_{solv\ water}$ kcal/mol | $\Delta G_{solv,\ ethanol}$ kcal/mol | $\Delta G_{sln,water}$ kcal/mol | $\Delta G_{sln,ethanol}$ kcal/mol |
|---|---|---|---|---|---|
| [RuCp(8-MTT-$\kappa S$)(PTA)$_2$] | -0.12 | -35.89 | -34.39 | -16.44 | -15.67 |
| [RuCp(8-MTT-$\kappa N7$)(PTA)$_2$] | 0 | -19.57 | -18.84 | 0 | 0 |
| [RuCp(8-MTT-$\kappa S$)(PPh$_3$)(mPTA)]$^+$ | -1.56 | -52.17 | -50.44 | -4.22 | -4.15 |
| [RuCp(8-MTT-$\kappa N7$)(PPh$_3$)(mPTA)]$^+$ | 0 | -49.51 | -47.85 | 0 | 0 |
| [RuCp(8-MTT-$\kappa S$)(mPTA)$_2$]$^{2+}$ | 5.72 | -148.84 | -144.07 | -1.39 | -1.08 |
| [RuCp(8-MTT-$\kappa N7$)(mPTA)$_2$]$^{2+}$ | 0 | -141.73 | -137.27 | 0 | 0 |

The complex [RuCp(8MTT-$\kappa S$)(PTA)$_2$] in gas phase is slightly more stable than the corresponding [RuCp(8MTT-$\kappa N7$)(PTA)$_2$] (small Gibbs energy difference of -0.12 kcal/mol). Solvation free energy in water is much more negative for the $\kappa S$- than for $\kappa N7$-coordination and probably for this reason the [RuCp(8MTT-$\kappa S$)(PTA)$_2$] is the synthesized complex in water. The energy difference between $\kappa S$- and $\kappa N7$-complexes decreases in approximately 0.8 kcal/mol in the less polar solvent ethanol. The origin of this large difference in solvation free energies in water lies on the different charge distribution in the two complexes and the resulting different dipole moment ([RuCp(8MTT-$\kappa S$)(PTA)$_2$] dipole moment = 15.73 D; [RuCp(8MTT-$\kappa N7$)(PTA)$_2$] = 7.1 D). Structural reasons could justify the dipole moments of the complexes. The electrostatic potential maps of both complexes (Figure 5) show that the negative potential is mainly located on carbonyl purine oxygen and nitrogen while positive electrostatic potential is distributed on the PTA ligands.
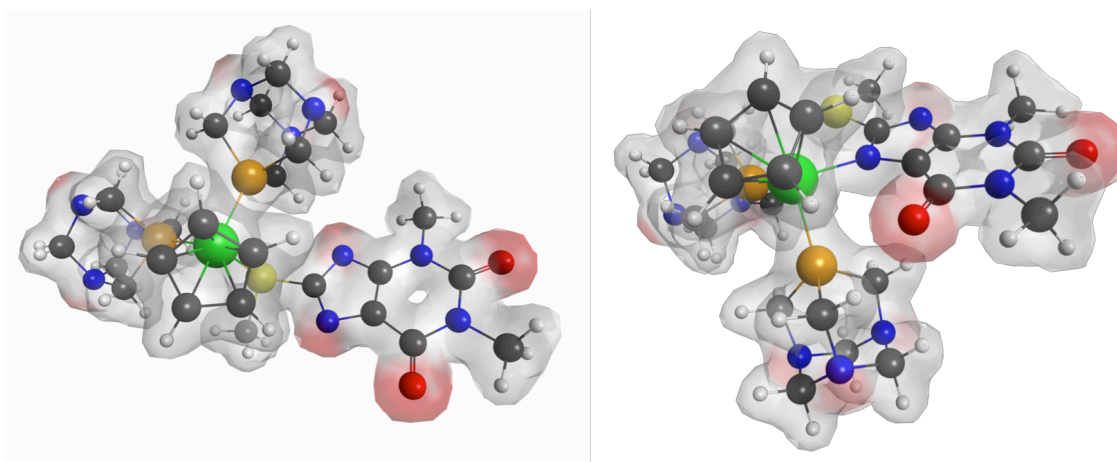
Figure 5. Molecular electrostatic potential superimposed over electronic isodensity surface for [RuCp(8MTT-κ*S*)(PTA)$_2$] (left) and [RuCp(8MTT-κ*N7*)(PTA)$_2$] (right). Isodensity surface corresponds to 0.02 au and the maximum electrostatic potential is 0.05 au.

In Table 5 Mulliken charges of selected atoms are shown. In gas phase, the distances between the O6 and O2 atoms to both P$_{PTA}$ atoms in [RuCp(8MTT-κ*S*)(PTA)$_2$] are (O6-P: 7.60 Å, 7.88 Å; O2-P: 8.67 Å, 10.33 Å) larger than those in [RuCp(8-MTT-κ*N7*)(PTA)$_2$] (O6-P: 3.26 Å, 5.72 Å; O2-P: 7,24 Å, 9.03 Å). Therefore, the binding of the 8MTT through the N7 atom approaches the purine ring to the PTA ligands and consequently, the κ*N7*-complex displays a dipolar moment (7.06 D) that is a 55% smaller than that for the κ*S*-complex. Consequently, the complex [RuCp(8-MTT-κ*S*)(PTA)$_2$] interaction with water-dipoles is stronger than that for [RuCp(8-MTT-κ*N7*)(PTA)$_2$], increasing the Gibbs free energy difference between each other and therefore favouring a larger stability of the more polar κ*S*-complex in water.

Table 5. Selected Mulliken charges for atoms of [RuCp(8-MTT-κ*S*)(PTA)$_2$] and [RuCp(8-MTT-κ*N7*)(PTA)$_2$].

| Atom | κ*S* | κ*N7* |
|------|------|-------|
| O2 | -0.422 | -0.416 |
| O6 | -0.395 | -0.467 |
| N7 | -0.271 | -0.352 |
| N9 | -0.330 | -0.276 |
| P1 | 0.634 | 0.622 |
| P2 | 0.595 | 0.518 |

A different result was obtained when the PTA ligands are replaced by the cationic mPTA. In gas phase the κ*N7*-8MTT-complex containing two mPTA is –5.72 kcal/mol more stable than the corresponding κ*S*-complex (Table 4). Nevertheless in polar solvents, the largest distance between negative charged purine oxygens and imidazolic nitrogens and positive charge on the mPTA in the 8MTT-κ*S*-complex makes solvation free energy lower than that of the corresponding κ*N7*-complex. The net effect produces that the mPTA-8MTT-κ*S*-complex is thermodynamically more stable in water and ethanol than the corresponding κ*N7*-complex. Similar results were obtained by the theoretical study of the ruthenium complexes containing the MTT and the cationic mPTA and the non-polar PPh$_3$. The κ*S*-complex in gas phase is more stable than the corresponding κ*N7*-complex by only -1.56 kcal/mol while in water this difference grows to -4.22 kcal/mol.

**Theoretical IR spectra**

The IR spectroscopy is a common and easy to use technique for characterizing metal complexes. Therefore the study of the theoretical IR spectra of the optimized complexes could provide an easy procedure for characterizing the coordination position of the 8MTT ligand in them. As a first conclusion, the study of the theoretical IR spectra of the complexes showed that the previously published assignation proposed for the purine C=O groups was erroneous. The

highest frequency adsorption band for purine C=O groups was traditionally assigned to $\nu$(C6=O) and the lowest to $\nu$(C2=O) [32] but the calculated IR spectra indicated that the highest frequency band is due to $\nu$(C2=O) and the lowest one at $\nu$(C6=O). The second important conclusion that could be extract is that unfortunately this technique is not useful to differentiate the coordination site of the thiopurine in this family of complexes. In Figure 6 is showed the calculated IR spectra of [RuCp(8-MTT-$\kappa$*N7*)(PPh$_3$)(mPTA)]$^+$ and [RuCp(8-MTT-$\kappa$*S*)(PPh$_3$)(mPTA)]$^+$ at B3LYP/DZVP level and the experimental spectra for the last one in the range from 1350 to 2000 cm$^{-1}$.
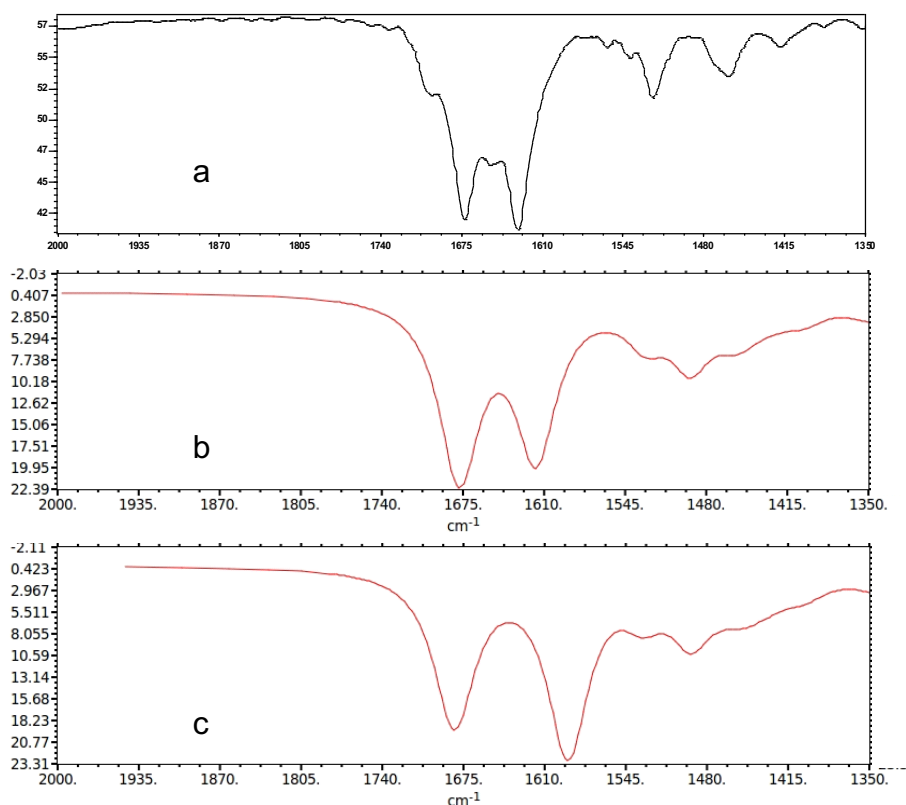


Figure 6. Experimental (a) and theoretical infrared spectra of [RuCp(8-MTT-$\kappa$*S*)(mPTA)(PPh$_3$)](CF$_3$OSO$_2$) (b) and theoretical of [RuCp(8-MTT-$\kappa$*N7*)(mPTA)(PPh$_3$)]$^+$ (c).

The most significant IR-absorption-frequencies of [RuCp(8MTT-$\kappa$*S*)(PPh$_3$)(mPTA)]$^+$ are in good agreement with experimental ones (IR cal:

$\nu$(C2=O) 1678 cm$^{-1}$, $\nu$(C6=O) 1617 cm$^{-1}$, $\nu$(C=C+C=N) 1528 cm$^{-1}$; IR exp: $\nu$(C2=O) 1673 cm$^{-1}$, $\nu$(C6=O) 1628 cm$^{-1}$, $\nu$(C=C+C=N) 1522 cm$^{-1}$). Similar bands for [RuCp(8-MTT-$\kappa N7$)(PPh$_3$)(mPTA)]$^+$ appears at 1681 cm$^{-1}$ ($\nu$(C2=O)), 1592 cm$^{-1}$ ($\nu$(C6=O)) and 1530 cm$^{-1}$ ($\nu$(C=C+C=N)). The strong similarity among the IR spectra of these complexes (Table 6) suggests that IR spectroscopy is not useful at all for differentiating the 8MTT-coordination site in these complexes.

Table 6. Calculated IR absorption frequencies (cm$^{-1}$) of the most significant bands of RuCp(8MTT-$\kappa S$)(mPTA)$_2$]$^{2+}$, [RuCp(8MTT-$\kappa N7$)(mPTA)$_2$]$^{2+}$, [RuCp(8MTT-$\kappa S$)(PTA)$_2$] and [RuCp(8MTT-$\kappa N7$)(PTA)$_2$]. Experimental frequencies are in parentheses.

| | [RuCp(8MTT-$\kappa S$)(mPTA)$_2$]$^{2+}$ | [RuCp(8MTT-$\kappa N7$)(mPTA)$_2$]$^{2+}$ | [RuCp(8MTT-$\kappa S$)(PTA)$_2$] | [RuCp(8MTT-$\kappa N7$)(PTA)$_2$] |
|---|---|---|---|---|
| $\nu$(C2=O) | 1696 (1672) | 1701 | 1683 (1690) | 1672 |
| $\nu$(C6=O) | 1600 (1598) | 1590 | 1642 (1636) | 1617 |
| $\nu$ (C=C+C=N) | 1534 (1521) | 1540 | 1519 (1536) | 1536 |

**Crystal structure of [RuCp(8-MTT-$\kappa S$)(PPh$_3$)(mPTA)](CF$_3$SO$_3$) (1).**

Single crystals good enough for determination of the X-ray structure of **1** were obtained by slow evaporation from its solution in EtOH. An ORTEP [33] view is displayed in Figure 7, the crystallographic data are given in Table 1 and a list of selected bond distances and angles appears in Table 7.
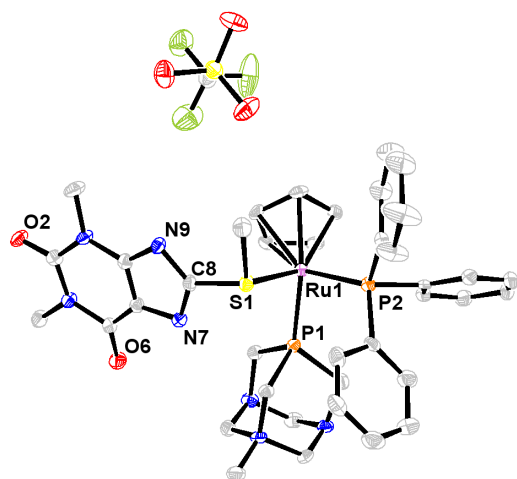
Figure 7. ORTEP view of **1** with atom numbering scheme showing 50 % probability thermal ellipsoids. For the sake of clarity the H atoms were omitted.

Table 7.  Experimental and calculated selected bond distances (Å) and Angles (deg) for **1**.

|  | **1** | B3LYP/DZVP |
|---|---|---|
| Ru1 – P1 | 2.2665(12) | 2.3752 |
| Ru1 – P2 | 2.2722(13) | 2.4092 |
| Ru1 – S1 | 2.3515(12) | 2.4722 |
| Ru1 – Cp(centroid) | 1.865(5) | 1,9370 |
| S1 – C9 | 1.808(5) | 1.8275 |
| S1 – C8 | 1.792(5) | 1.7887 |
| C8t – N7 | 1.308(7) | 1.3320 |
| C8t – N9 | 1.376(6) | 1.3606 |
| P1P – C3P | 1.856(10) | 1.8799 |
|  |  |  |
| P1 – Ru1 – P2 | 94.17(5) | 96.106 |
| P1 – Ru1 – S1 | 90.18(4) | 93.454 |
| P2 – Ru1 – S1 | 89.32(4) | 91.425 |
| C8 – S1 – Ru1 | 113.00(17) | 106.175 |
| C9 – S1 – Ru1 | 109.72(18) | 110.637 |
| S1 – C8 – N7 | 122.9(4) | 124,427 |
| S1 – C8 – N9 | 116.8(4) | 117.244 |

The asymmetric unit is constituted by the chiral cation complex [RuCp(8-MTT-κ$S$)(PPh$_3$)(mPTA)]$^+$ and a CF$_3$SO$_3^-$ anion. The complex unit is made of an octahedral-distorted ruthenium coordinated to a η$^5$-Cp, a 8-MTT by the S atom, and to a PPh$_3$ and mPTA molecules by the P atoms. The Ru-Cp$_{centroid}$ bond length is 1.8748(1) Å that is similar than that for [RuCpI (PPh$_3$)(mPTA)](CF$_3$SO$_3$) (Ru-Cp$_{centroide}$: 1.834 Å) [10] but larger than that found in starting complex [RuCpCl(PPh$_3$)(mPTA)](CF$_3$SO$_3$) (Ru-Cp$_{centroide}$: 1.834 Å) [34]. The distances between the metal and the P$_{mPTA}$ and P$_{PPh_3}$ atoms (Ru-P1: 2.2755(14) Å; 2.3097(14) Å) are similar to that observed for similar complexes and very similar than those for starting complex (Ru-P: 2.262(3) Å; 2.300(3) Å) [10,39].

Although there are numerous examples of thioethers bonded by S to Ru, there are only four examples containing NCS-thioether two of them with a N-pyridine: [Ru(dps-N,N')$_2$pmprs](PF$_6$)$_2$, [Ru($N,N$-dps)$_2$($N,S$-c)](PF$_6$)$_2$ and [Ru($N,N$-dps)$_2$($N,S$-dps)](PF$_6$)$_2$ (dps = di-2-pyridyl sulfide; c = 2-pyridymethyl 2-pyridyl sulfide; pmprs = 4-methylpyrimidin-2-yl 2-pyridylmethyl sulphide) and [Ru($N,N$-dps)$_2$($N,S$-c)][PF$_6$]$_2$·C$_3$H$_6$O (Ru-S = 2.370(1) Å) [35], and the parent complex [RuCp(8-MTT-κ$S$)(PTA)$_2$] [11]. The distances Ru-S1 (2.3518(13) Å), C8-S1 (1.755(4) Å) and S1-CH$_3$ (1.804(4) Å) in **1** are similar than those for parent ruthenium complex [RuCp(8-MTT-κ$S$)(PTA)$_2$] (Ru-S1 = 2.3515(12) Å; S1t-C8t = 1.792(5) Å; S1t-C9t = 1.808(5) Å)). Also the bond lengths between C8 and the imidazolic nitrogen atoms N7 (1.328(5) Å) and N9 (1.365(5) Å) in **1** are practically identical to those found in [RuCp(8-MTT-κ$S$)(PTA)$_2$] (C8t-N7t = 1.309(7) Å; C8t-N9t = 1.376(6) Å), as well as the rest of distances and angles into the purine molecule. This fact is in agreement with a delocalization of the electrons in the skeleton of the purine ligand but they are mainly located between the N7-C8-S-Ru atoms. This supposition was supported by the preformed theoretical calculation discussed previously. The electrons coming from the deprotonation of the N7 atom are also on the S8 atom, the donor site of the ligand.

The purine is basically planar and positioned near the less bulky ligand, the mPTA (angle cone for mPTA = ~102 °; cone angle for PPh$_3$ = ~ 147 °) [36] and perpendicularly to it (Figure 8). The remaining distances and angles are similar

to those found in other metal purine complexes containing phosphines [37]. Finally, the distance between close molecules is larger than 3.00 Å, indicating that there are not significant interactions between them but interestingly the distance between purines in the packing is 3.4 Å the same that separate the purines in the DNA.
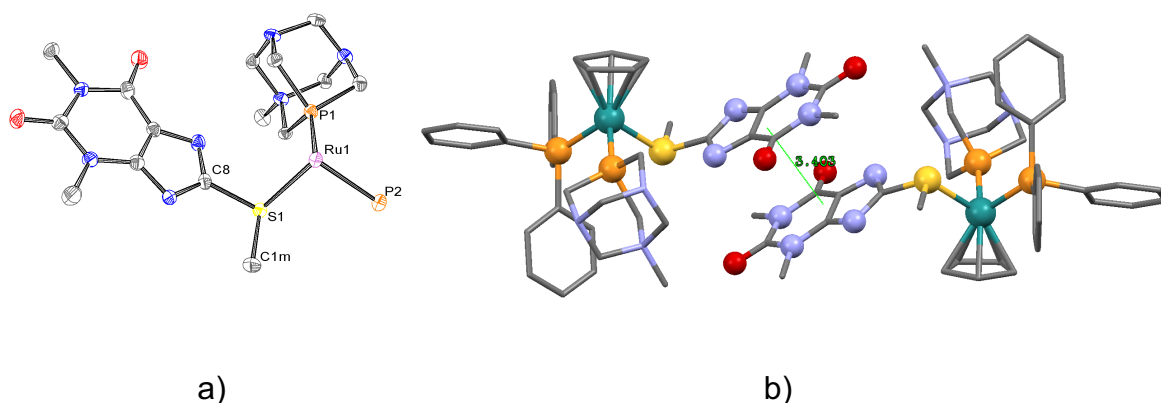


a)                                                      b)

Figure 8. a) View of compound **1**. PPh₃, Cp and H atoms were omitted for the sake of clarity. b) Packing of two molecules of **1**.


**Crystal structure of [RuCp(8-MTT-κ*S*)(mPTA)₂]Cl(CF₃SO₃)·1.5H₂O (2·1.5H₂O).**

Single crystals suitable for X-ray analysis of **2·1.5H₂O** were obtained by slow evaporation from its water solution. An ORTEP [40] view is displayed in Figure 9, the crystallographic data are given in Table 1 and a list of selected bond distances and angles appears in Table 8.


Table 8. Selected experimental Bond Distances (Å) and Angles (deg) for **2a** and **2b.** Calculated data for optimized structure of **2** are included.

|  | 2a | 2b | B3LYP structure |
|---|---|---|---|
| Ru1(2) – P1 | 2.256(2) | 2.268(2) | 2.3317 |
| Ru1(2) – P2 | 2.280(2) | 2.267(2) | 24019 |
| Ru1(2) – S10 | 2.374(2) | 2.365(2) | 2.4775 |
| Ru1(2)-Cp(centroid) | 1.861(3) | 1.869(3) | 1.9310 |

| | | | |
|---|---|---|---|
| S10 – C10 | 1.824(10) | 1.793(8) | 1.8335 |
| S10 – C8 | 1.780(9) | 1.761(9) | 1.7873 |
| C8 – N7 | 1.326(11) | 1.325(11) | 1.3318 |
| C8 – N9 | 1.365(11) | 1.383(11) | 1.3560 |
| P1 – Ru1(2) – P2 | 99.41(9) | 95.06(9) | 97.93 |
| P1 – Ru1(2) – S10 | 91.24(8) | 91.75(8) | 88.69 |
| P2 – Ru1(2) – S10 | 89.56(8) | 93.08(8) | 90.89 |
| C8 – S10 – Ru1(2) | 107.4(3) | 108.3(3) | 105.83 |
| C10 – S10 – Ru1(2) | 109.5(4) | 109.9(3) | 112.65 |
| S10 – C8 – N7 | 116.1(6) | 124.1(7) | 118.59 |
| S10 – C8 – N9 | 125.6(7) | 117.8(7) | 122.17 |

The asymmetric unit contains 1.5 disordered molecules of $H_2O$, two $Cl^-$ and two $CF_3SO_3^-$ anions, and two cationic [RuCp(8-MTT-κ$S$)(mPTA)$_2$] isomers (**2a**, **2b**). The two isomers are constituted by a ruthenium coordinated with a slightly distorted pseudo-octahedral geometry to one $\eta^5$-Cp, two mPTA ligands bonded by the P atom and one 8-MTT ligand through the S atom. The main difference between both isomers is about the relative disposition of the purine. In the isomer **2a** the purine moiety disposes its O6 atom close to an mPTA while in the isomer **2b** this oxygen atom is as far as possible from the phosphines. Interestingly, the distortion of the coordination geometry in **2a** (P1A-Ru1-P2A = 99.41(9)°; P1A-Ru1-S10A = 91.24(8)°; P2A-Ru1-S10A = 89.56(8)°) is larger than in **2b** (P1B-Ru2-P2B = 95.06(9)°; P1B-Ru2-S10B = 91.75(8)°; P2B-Ru2-S10B = 93.08(8)°) but in both complexes is shorter than in the starting complex [RuClCp(mPTA)$_2$](CF$_3$SO$_3$)$_2$ (P1-Ru1-P2 = 99.44(4)°; P1-Ru1-Cl1 = 84.55(5)°; P2-Ru1-Cl1 = 87.04(5)°) [39]. The distances between purine and the rest of ligands in the complex are larger than 3 Å and therefore there are not any strong interaction between purine and the rest of the complex molecules in both isomers. Therefore, the shorter geometrical distortion in both isomers with respect to the starting complex [RuCpCl(mPTA)$_2$](CF$_3$SO$_3$)$_2$ is only able to be attributed to the effect of the 8-MTT ligand on the electronic allocation into the complex molecule. Calculations performed with crystallographic initial structure of **2b** converged into **2a**, showing that this is the most stable isomer in gas

phase. Therefore, the presence of both isomers in the crystal cell should be probably a requirement of the crystal packing.
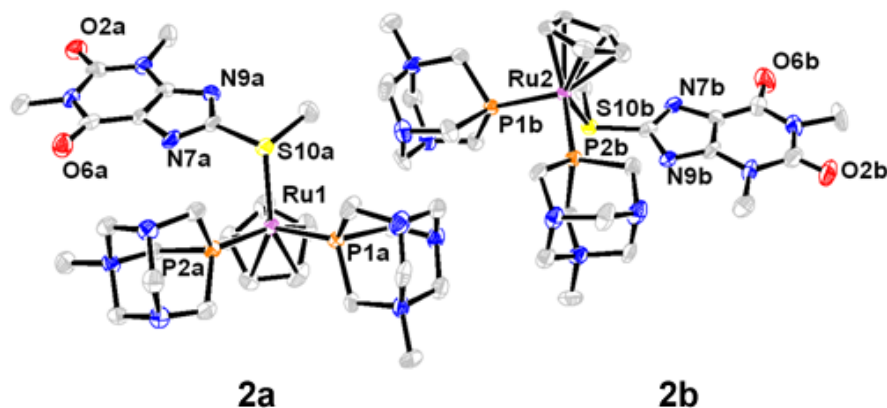


Figure 9. View of the two isomers constituting **2**. For the sake of clarity the H atoms were omitted.

The Ru-Cp$_{centroid}$ (**2a**: 1.861 Å; **2b**: 1.869 Å) distances and bond lengths Ru-P$_{mPTA}$ (Ru1-P1A = 2.256(2) Å; Ru1-P2A = 2.280(2) Å; Ru2-P1B = 2.268(2) Å; Ru1-P2A = 2.267(2) Å) for the two isomers are similar and larger than the corresponding ones in the starting complex (Ru-Cp$_{centroid}$ = 1.840 Å; 2.2509(12) Å and 2.2599 (3) Å). The complex **2** supports that the previously unexpected coordination mode of the 8MTT ligand by the S atom should be considered as a natural reactivity position for thioether-purines as predicted by the theoretical studies presented previously. Therefore, it is possible targeted the coordination position of the 8MTT and possibly of the thiopurines by choosing the adequate metal moiety.

The Ru-S distances are similar in both isomers **2a** (Ru1-S10A = 2.374(2) Å) and **2b** (Ru2-S10B = 2.365 (2) Å) and larger than that in parent complex [RuCp(8-MTT-κS)(PTA)$_2$] [11] (Ru1-S1t = 2.3515(12) Å) and [Ru(dps-N,N')$_2$pmprs](PF$_6$)$_2$·C$_2$H$_3$N (Ru1-S34 = 2.3581(13) Å) [40a] (dps = di-2-pyridyl sulphide; c = 2-pyridymethyl 2-pyridyl sulphide; pmprs = 4-methylpyrimidin-2-yl

2-pyridylmethyl sulphide), but similar to those found in [Ru($N,N$-dps)$_2$($N,S$-c)][PF$_6$]$_2$·C$_3$H$_6$O (Ru-S = 2.370(1) Å) [40b], and still shorter than that in [Ru($N,N$-dps)$_2$($N,S$-dps)](PF$_6$)$_2$·H$_2$O (Ru-S(3) = 2.424(2) Å). The C8-S1 and S1-CH$_3$ distances in both isomer complexes (C8A-S10A = 1.780(9) Å; S10A-CH$_3$ = 1.824(10) Å; C8B-S10B = 1.761(9) Å; S10B-CH$_3$ = 1.793(8) Å) are larger than those found in parent complex [RuCp(8-MTT-κ$S$)(PTA)$_2$] (C8-S1 = 1.755(4) Å; S1-CH$_3$ = 1.770(5) Å). The bond lengths between C8 and the imidazolic nitrogen atoms N7 and N9 in **2a** and **2b** are quite different (C8A-N7A = 1.326 (11) Å; C8A-N9A = 1.365(11) Å; C8B-N7B = 1.325(11) Å; C8B-N9B = 1.383(11) Å) like that observed for [RuCp(8-MTT-κ$S$)(PTA)$_2$], and as suggested for the calculation and parent complexes, it is in agreement with the electrons in the skeleton of complex **2** mainly located between the N7-C8-S-Ru atoms, with a particular high density charge on the N7-C8 and on the S-Ru bond.

The purines in both isomers are planar and their angle with the Cp is 31.66º (**2a**) and 28.60º (**2b**), which are quite different to that found in parent complex [RuCp(8-MTT-κ$S$)(PTA)$_2$] (4.14º). The 8MTT disposition avoids repulsive interactions with the rest of the molecule, as the distances among the purine and the others ligands in the complex are longer than 3 Å. A 3D network thought extensive hydrogen bonding involving the disordered H$_2$O molecule, the N7, N9, O6 and Cl atoms forms the crystal lattice structure (Figure 10). It is interesting to stress that the bond distance C6-O6 in both isomers is significantly different. For **2b**, in which the O6 is bonded by a clear hydrogen bond to a water molecule, the distance C7-O3 (1.253(11) Å) is larger than that in **2a** (1.245(11) Å). A similar effect is observed for the bond distances in purine imidazolic ring of both isomers, which are linked by a strong hydrogen bond to the N9A in **2a** (C4A-N9A = 1.335(11) Å; C4B-N9B = 1.345(11) Å) and to the N7B in **2b** (C5B-N7B = 1.403(11) Å; C5A-N7A = 1.379(11) Å).
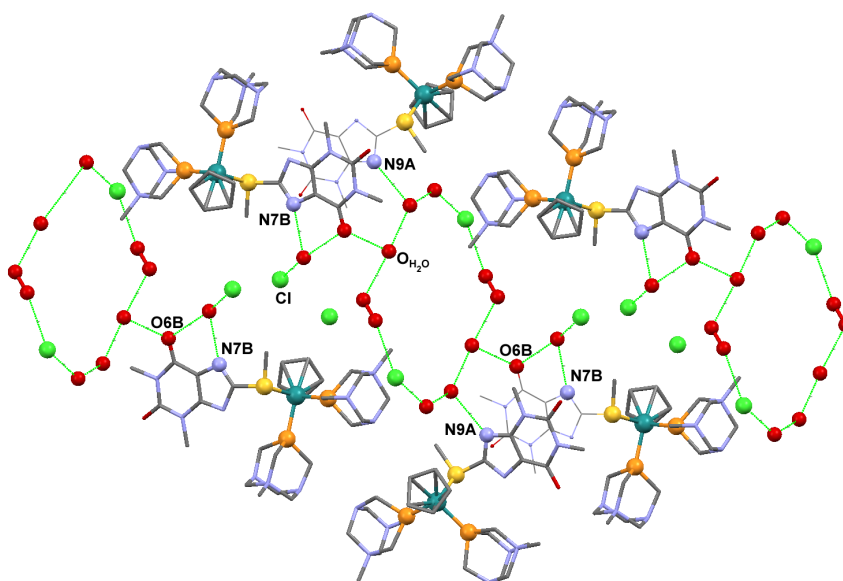
Figure 10. Hydrogen bond network produced by the interaction of the disordered $H_2O$ molecule, the N7, N9, O6 and Cl atoms in **2·1.5H₂O**.

## Conclusion

Structures, infrared spectra and thermodynamical properties in the gas phase and in water and ethanol solution of the complexes [RuCp(8MTT-κ*S)*LL'] and [RuCp(8MTT-κ*N7)*LL'] have been investigated by DFT theoretical methods at B3LYP/DZVP level of theory. The theoretical studies show that the complexes containing the 8MTT-ligand bonded by the S atom are more stable in water and EtOH that those bonded by the N7 atom while in gas-phase the stability of both isomers tend to be the same as the phosphine is more positively charged. The stability of the complexes in water is justified by the larger interaction of the water molecules with the more polar ruthenium coordinated 8MTT-κ*S*- ligand. The calculate IR spectra for the complexes showed: i) the traditional assignation for the purine *C*=O absorption bands was erroneous; ii) it is not possible to determine the coordination position of the 8MTT-ligand by the IR spectroscopy. The obtained theoretical results are in agreement with obtained until now experimental results as two new thiopurine-κ*S*-complexes, [RuCp(8MTT-κ*S*)(mPTA)(PPh₃)](CF₃OSO₂) (**1**) and [RuCp(8MTT-κ*S*)(mPTA)₂]Cl(CF₃OSO₂)·1.5H₂O (**2·1.5H₂O**) were synthesized and characterized by single crystal X-ray diffraction. Therefore, this initially strange

coordination mode of a thioether for the 8MTT ligand is natural when it is coordinate to a metal moiety as the {RuCpLL'} that leads to the formation of a dipolar moment into the purine molecule. Studies are focused to determine if the -κ*S*-coordination mode is the general interaction of thioethers and {RuCpLL'}, which could provide new metal-κ*S*-coordination-thioethers complexes with biological properties and also with possible valuable properties for catalysing the transformation of thio-ethers in water.

**Supporting Information Available:** Crystallographic data for the structures in this paper have been deposited with the Cambridge Crystallographic Data Centre as supplementary publications nos. CCDC 944487-944488. Copies of the data can be obtained, free of charge on applications to CCDC, 12 Union Road, Cambridge CB2 1EZ, UK, (fax: +44 1223 336033 or e-mail: deposit@ccdc.cam.ac.uk). Geometries corresponding to optimized structures of 8MTTH, 8MTT and κ*S*- and κ*N7*-8MTT complexes are included in supporting information. Plots of HOMO and LUMO and theoretical infrared spectra are also included.

**References**

[1] (a) W.A. Wani, S. Prashar, S. Shreaz, S. Gómez-Ruiz, Coord. Chem. Rev. 312 (2016) 67; (b) J. Furrer, G. Süss-Fink, Coord. Chem. Rev. 309 (2016) 36; (c) S. K. Singha, D. S. Pandey, Adv. 4 (2014) 1819; (d) E. Guerrero, S. Miranda, S. Lüttenberg, N. Fröhlich, J.-M. Koenen, F. Mohr, E. Cerrada, M.

Laguna, A. Mendía, Inorg. Chem. 52 (2013), 6635; (e) S. Miranda, E. Vergara, F. Mohr, D. de Vos, E. Cerrada, A. Mendía, M. Laguna, Inorg. Chem. 47 (2008) 5641; (f) E. Vergara, S. Miranda, F. Mohr, E. Cerrada, E. R. T. Tiekink, P. Romero, A. Mendía, M. Laguna, Eur. J. Inorg. Chem. (2007) 2926; (g) F. Mohr, S. Sanz, E. R. T. Tiekink, M. Laguna, Organometallics 25 (2006) 3084; (h) B.S. Howerton, D.K. Heidary, E.C. Glazer, J. Am. Chem. Soc. 134 (2012) 8324; (i) K.J. Kilpin, C. M. Clavel, F. Edafe, P.J. Dyson, Organometallics 31 (2012) 7031; (j) M. Carreira, R. Calvo-Sanjuán, M. Sanaú, I. Marzo, M. Contel, Organometallics 31 (2012) 5772; (k) T. Mihály, M. Garijo-Añorbe, F. Albertí, P.J. Sanz-Miguel, B. Lippert, Inorg. Chem. 51 (2012) 10437; (l) H-C. Tai, R. Brodbeck, J. Kasparkova, N.J. Farrer, V. Brabec, P.J. Sadler, R.J. Deeth, Inorg. Chem. 51 (2012) 6830; (m) R. Gaur, L. Mishra, Inorg. Chem. 51 (2012) 3059; (n) J. Vícha, G. Demo, R. Marek, Inorg. Chem. 51 (2012) 1371.

[2] B. Rosenberg, L. van Camp, T. Krigas, Nature 205 (1965) 698.

[3] E.R. Jamieson, S.J. Lippard, Chem. Rev. 99 (1999) 2467.

[4] (a) B. Stordal, M. Davey, IUBMB Life 59 (2007) 696; (b) N. Pabla, Z. Dong, Kidney Int. 73 (2008) 994.

[5] (a) S. Betanzos-Lara, L. Salassa, A. Habtemariam, P.J. Sadler, Chem. Commun. (2009) 6622; (b) G.I. Pascu, A.C.G. Hotze, C. Sanchez-Cano, B.M. Kariuki, M.J. Hannon, Angew. Chem., Int. Ed. 46 (2007) 4374; (c) W.H. Ang, P.J. Dyson, Eur. J. Inorg. Chem. (2006) 4003; (d) Y. K. Yan, M. Melchart, A. Habtemariam, P.J. Sadler, Chem. Commun. (2005) 4764; (e) A.C.G. Hotze, S.E. Caspers, D. de Vos, H. Kooijman, A.L. Spek, A. Flamigni, M. Bacac, G. Sava, J.G. Haasnoot, J.J. Reedijk, Biol. Inorg. Chem. 9 (2004) 354; (f) R.E. Morris, P.J. Sadler, H. Chen, D. Jodrell, US Pat. 6 750 251 B2 (2004).

[6] (a) E. Alessio, G. Mestroni, A. Bergamo, G. Sava, Curr. Top. Med. Chem. 4 (2004) 1525; (b) E. Alessio, G. Mestroni, A. Bergamo, G Sava, Met. Ions Biol. Syst. 42 (2004) 323.

[7] C.G. Hartinger, S. Zorbas-Selfried, M.A. Jakupee, B. Kynast, H. Zorbas, B.K.J. Keppler, Inorg. Biochem. 100 (2006) 891.

[8] A. Romerosa, P. Bergamini, V. Bertolasi, A. Canella, M. Cattabriga, R. Gavioli, S. Mañas, N. Mantovani, L. Pellacani, Inorg. Chem. 43 (2004) 905.

[9] P. Bergamini, V. Bertolasi, L. Marvellli, A. Canella, R. Gavioli, N. Mantovani, S. Mañas, A. Romerosa, Inorg. Chem. 46 (2007) 4267.

[10] A. Romerosa, T. Campos-Malpartida, C. Lidrissi, M. Saoud, M. Serrano-Ruiz, M. Peruzzini, J.A. Garrido-Cardenas, F. Garcia-Maroto, Inorg. Chem. 45 (2006) 1289.

[11] L. Hajji, C. Saraiba-Bello, A. Romerosa, G. Segovia-Torrente, M. Serrano-Ruiz, P. Bergamini, A. Canella, Inorg. Chem. 50 (2011) 873.

[12] A. Altomare, G. Cascarano, C. Giacovazzo, A. Guagliardi, M. C. Burla, G. Polidori, M.J. Camalli, Appl. Crystallogr. 27 (1994) 435.

[13] G. M. Sheldrick, SHELXTL vesion 6.14, Bruker-AXS, Madison, W1, USA, 2003.

[14] M. W. Schmidt, K.K. Baldridge, J.A. Boatz, S.T. Elbert, M.S. Gordon, J.H. Jensen, S. Koseki, N. Matsunaga, K.A. Nguyen, S.J. Su, R.L. Windus, M. Dupuis, J.A.J. Montgomery, Comput. Chem. 14 (1993) 1347.

[15] M.S. Gordon, M.W. Schmidt; C. E. Dykstra, G. Frenking, K.S. Kim, G.E. Scuseria (Eds.). In Theory and Applications of Computational Chemistry: The First Forty Years. Elsevier, Amsterdam, 2005, 1167.

[16] A. D. J. Becke, Chem. Phys. 98 (1993) 5648

[17] C. Lee, W. Yang, R.G. Parr, Phys. Rev. B 37 (1988) 785.

[18] N. Godbout, D.R. Salahub, J. Andzelm, E. Wimmer, Can. J. Chem. 70 (1992) 560.

[19] Avogadro: an open-source molecular builder and visualization tool. Version 1.00. http://avogadro.openmolecules.net/

[20] R. Krishnan, J.S. Binkley, R. Seeger, J.A. Pople, J. Chem. Phys. 72 (1980) 650.

[21] J-P. Blaudeau, M.P. McGrath, L.A. Curtiss, L. Radom, J. Chem. Phys. 107 (1997) 501.

[22] T. Clark, J. Chandrasekhar, PV.R. Schleyer, J. Comp. Chem. 4 (1983) 294.

[23] J. Tomasi, Theor. Chem. Acc. 112 (2004) 184.

[24] J. Tomasi, B. Mennucci, R. Cammi, Chem. Rev. 105 (2005) 2999.

[25] V. Barone, M.J. Cossi, Phys. Chem. A. 102 (1998) 1995.

[26] B. Curchod, F. Rotzinger, Inorg. Chem. 50 (2011) 8728.

[27] J. Ho, A. Klamt, M.L. Coote, J. Phys. Chem. A. 114 (2010) 13442.

[28] D. Russell Johnson III (Ed.). NIST Computational Chemistry Comparison and Benchmark Database. NIST Standard Reference Database Number 101. Release 15b. http://cccbdb.nist.gov/. 2011,

[29] B. M. Bode, M.S.J. Gordon, Graphics Mod. 16 (1998) 133.

[30] http://www.chemissian.com.

[31] B.D. Alexander, T.J. Dines, R.W. Longhurst, Chem. Phys. 352 (2008) 19.

[32] E. Colacio, A. Romerosa, J. Ruiz, P. Roman, J.M. Gutiérrez-Zorrilla, A. Vegas, M. Martínez-Ripoll, Inorg. Chem. 50 (2011) 873.

[33] C. K. Johnson, ORTEP II. Report ORNL-5138, Oak Ridge National Laboratory, Oak Ridge, TN. 1976.

[34] B. González, P. Lorenzo-Luis, P. Gili, A. Romerosa, M. Serrano-Ruiz, J. Organomet. Chem. 694 (2009) 2029.

[35] (a) L. Baradello, S. Lo Schiavo, F. Nicolo, S. Lanza, G. Alibrandi, G. Tresoldi, F. Nicolo, S. Lanza, Acta Crystallogr., Sect.C: Cryst. Struct. Commun. C62 (2005) m169; (b) L. Baradello, S. Lo Schiavo, F. Nicolo, S. Lanza, G. Alibrandi, G. Tresoldi, Eur. J. Inorg. Chem. (2004) 3358; (c) R. Scopelliti, G. Bruno, C. Donato, G. Tresoldi, Inor. Chim. Acta 313 (2001) 43.

[36] C.A. Tolman, J. Am. Chem. Soc. 92 (1970) 2956; (b) J.R. Delerno, L.M. Trefonas, M.Y. Darensbourg, R.J. Majeste, Inorg. Chem. 15 (1976) 816.

[37] Cambridge Crystallographic Data Centre (CCDC), 2015 (http://www.ccdc.cam.ac.uk/Community/Depositastructure/pages/DepositaStructure.aspx).